

# An explicit scheme for multifluid magnetohydrodynamics

Stephen O’Sullivan<sup>1</sup> <sup>\*</sup> and Turlough P. Downes<sup>2</sup>

<sup>1</sup>UCD School of Mathematical Sciences, University College Dublin, Belfield, Dublin 4, Ireland

<sup>2</sup>School of Mathematical Sciences, Dublin City University, Glasnevin, Dublin 9, Ireland

Accepted ..... Received ..... ; in original form .....

## ABSTRACT

When modeling astrophysical fluid flows, it is often appropriate to discard the canonical magnetohydrodynamic approximation thereby freeing the magnetic field to diffuse with respect to the bulk velocity field. As a consequence, however, the induction equation can become problematic to solve via standard explicit techniques. In particular, the Hall diffusion term admits fast-moving whistler waves which can impose a vanishing timestep limit.

Within an explicit differencing framework, a multifluid scheme for weakly ionised plasmas is presented which relies upon a new approach to integrating the induction equation efficiently. The first component of this approach is a relatively unknown method of accelerating the integration of parabolic systems by enforcing stability over large compound timesteps rather than over each of the constituent substeps. This method, Super Time Stepping, proves to be very effective in applying a part of the Hall term up to a known critical value. The excess of the Hall term above this critical value is then included via a new scheme for pure Hall diffusion.

**Key words:** MHD – shockwaves – methods: numerical – ISM: clouds – dust, extinction

## 1 INTRODUCTION

Dynamically important magnetic fields are commonplace in astrophysics. In many cases, where these fields interact with fluids, researchers have assumed that the equations of ideal magnetohydrodynamics (MHD) are sufficient in modeling the evolution of the magnetic fields and the fluids with which they interact. There are clear examples, however, where the assumptions underpinning the equations of ideal MHD are not valid. In dense molecular clouds, for example, the density of charged particles can be much lower than that of the neutral species (Ciolek & Roberge 2002, hereafter CR02). Under these conditions, coupling between the motions of the fluids and the magnetic field is not perfect, and diffusive effects become significant. Similarly, ideal MHD is not believed to be valid in accretion disks around young stellar objects (Wardle 2004). The latter point is particularly interesting given the importance attached to the interaction between accretion disks and magnetic fields in the launching of stellar jets and outflows (e.g. Shu et al. 1994; Fendt & Camenzind 1996; Ouyed, Pudritz & Stone 1997; Lery et al. 1999; Ferreira 2004). When modeling systems such as these therefore, a full multifluid treatment permit-

ting relative motions between different component species should be adopted.

Many authors (Tóth 1994; Smith & Mac Low 1997; Stone 1997; Chieze, Pineau des Forets & Flower 1998) have suggested schemes for numerically integrating the multifluid equations in the limit of pure ambipolar diffusion. In this regime the charged species are firmly tied to the magnetic field lines as they diffuse through the neutral gas. The problem becomes more technically challenging, however, when charged species may be loosely attached to the field lines and Hall diffusion can become important. Notably, it is thought that Hall diffusion may play an important role in environments such as the surfaces of neutron stars (Hollerbach & Rüdiger 2004), protostellar disks (Wardle 2004), and dense molecular clouds (CR02).

In their numerical studies of molecular clouds, CR02 assumed that the ionisation fraction is low and that the inertia of the charged particles may be neglected. They were then able to integrate the governing equations for a multifluid problem including the presence of several species of charge-carrying grain. Separately, Sano & Stone (2002a; 2002b) performed multifluid calculations designed to examine the Hall effect in the context of the magnetorotational instability in accretion disks. However, both of the schemes used by these authors are subject to a rather stringent stability criterion which requires that the timestep tends to zero as the Hall effect becomes large (Falle 2003, hereafter F03).

<sup>\*</sup> E-mail: stephen.osullivan@ucd.ie (SOS); turlough.downes@dcu.ie (TPD)

To circumvent this constraint F03 presents a scheme employing an implicit method of integrating the magnetic field equation. This has the advantage of allowing timesteps up to the limit dictated by the hyperbolic components of the equations. However, since large scale multifluid simulations are of obvious interest, the inherent difficulty of parallelising implicit schemes becomes a serious disadvantage.

In this work we present a fully explicit numerical scheme for solving the multifluid equations describing a weakly ionised plasma. The usual stability restrictions are relaxed through a combination of a technique known as Super Time Stepping (STS) (Alexiades, Amiez & Gremaud 1996) and a new method which we call the Hall Diffusion Scheme (HDS). Crucially, since the scheme is explicit, it is straightforward to parallelise and to implement on top of an adaptive mesh refinement (AMR) engine.

In Section 2 the governing equations are described; Section 3 contains a detailed description and analysis of the numerical scheme; Section 4 contains numerical tests demonstrating the reliability of the scheme; and in Section 5 the relevance of this work is discussed.

## 2 THE MULTIFLUID EQUATIONS

We assume a weakly ionised plasma such that the mass density is dominated by the neutral component of the gas. Then, relative to the scale-length of the system, if particles of a given charged species have small mean free paths in the neutral gas, or small Larmor radii, their pressure and inertia may be neglected.

For convenience it is assumed there is no mass transfer between species. It is straightforward, however, to insert the necessary terms for a more general treatment to include mass transfer (for example, see F03 and CR02) if desired. The equations governing the evolution of the multifluid system (CR02; F03) can then be written as

$$\frac{\partial \rho_i}{\partial t} + \frac{\partial}{\partial x} (\rho_i \mathbf{q}_i) = 0, \quad (1)$$

$$\frac{\partial \rho_1 \mathbf{q}_1}{\partial t} + \frac{\partial}{\partial x} (\rho_1 u_1 \mathbf{q}_1 + p_1 \mathbf{I}) = \mathbf{J} \times \mathbf{B}, \quad (2)$$

$$\frac{\partial e_1}{\partial t} + \frac{\partial}{\partial x} \left[ u_1 \left( e_1 + p_1 + \frac{1}{2} \rho_1 q_1^2 \right) \right] = \mathbf{J} \cdot \mathbf{E} + \sum_{i=1}^N H_i, \quad (3)$$

$$\frac{\partial \mathbf{B}}{\partial t} + \frac{\partial \mathbf{M}}{\partial x} = \frac{\partial}{\partial x} \mathbf{R} \frac{\partial \mathbf{B}}{\partial x}, \quad (4)$$

$$\alpha_i \rho_i (\mathbf{E} + \mathbf{q}_i \times \mathbf{B}) + \rho_i \rho_1 K_{i1} (\mathbf{q}_1 - \mathbf{q}_i) = 0, \quad (5)$$

$$H_i + G_{i1} + \alpha_i \rho_i \mathbf{q}_i \cdot \mathbf{E} = 0, \quad (6)$$

$$\frac{\partial B_x}{\partial x} = 0, \quad (7)$$

$$\sum_{i=2}^N \alpha_i \rho_i = 0, \quad (8)$$

$$\sum_{i=2}^N \alpha_i \rho_i \mathbf{q}_i = \mathbf{J}. \quad (9)$$

The subscripts denote the species, with a subscript of 1 indicating the neutral fluid. The variables  $\rho_i$ ,  $\mathbf{q}_i \equiv (u_i, v_i, w_i)^T$  and  $p_i$  are the mass density, velocity and pressure of species  $i$ . The identity matrix, current density and magnetic flux density are represented by  $\mathbf{I}$ ,  $\mathbf{J}$ ,  $\mathbf{B}$  respectively.  $K_{i1}$  describes the collisional interaction between species  $i$  and the neutral fluid,  $\alpha_i$  is the charge-to-mass ratio for species  $i$ ,  $G_{i1}$  is the energy transfer rate from species  $i$  to the neutral fluid,  $H_i$  is the energy source or sink appropriate to species  $i$ ,  $\mathbf{R}$  is the resistivity matrix and  $\mathbf{M}$  is the hyperbolic flux of  $\mathbf{B}$ . See F03 and CR02 for a more detailed description of these terms. Note that in general  $K_{i1}$  and  $G_{i1}$  may depend on the temperatures and relative velocities of the interacting species. Equations (1) to (6) are the equations governing the conservation of mass, neutral momentum, neutral energy, magnetic flux, charged momentum, and charged energy. Equations (7) to (9) describe the divergence of  $\mathbf{B}$ , charge neutrality, and current respectively.

From Faraday's law in one dimension  $\partial B_x / \partial t = 0$  so that the trivial  $B_x$  component may be dropped from equation (4). The hyperbolic flux is then

$$\mathbf{M} = (u_1 B_y - v_1 B_x, u_1 B_z - w_1 B_x) \quad (10)$$

and the resistivity matrix is

$$\mathbf{R} = \begin{pmatrix} (r_O - r_A) \frac{B^2}{B^2} + r_A & (r_A - r_O) \frac{B_y B_z}{B^2} + r_H \frac{B_x}{B} \\ (r_A - r_O) \frac{B_y B_z}{B^2} - r_H \frac{B_x}{B} & (r_O - r_A) \frac{B_y}{B^2} + r_A \end{pmatrix} \quad (11)$$

where  $r_O$ ,  $r_H$  and  $r_A$  are the Ohmic, Hall and ambipolar resistivities respectively and are defined by

$$r_O = \frac{1}{\sigma_O}, \quad (12)$$

$$r_H = \frac{\sigma_H}{\sigma_H^2 + \sigma_A^2}, \quad (13)$$

$$r_A = \frac{\sigma_A}{\sigma_H^2 + \sigma_A^2}, \quad (14)$$

with conductivities

$$\sigma_O = \sum_{i=2}^N \alpha_i \rho_i \beta_i, \quad (15)$$

$$\sigma_H = \frac{1}{B} \sum_{i=2}^N \frac{\alpha_i \rho_i}{1 + \beta_i^2}, \quad (16)$$

$$\sigma_A = \frac{1}{B} \sum_{i=2}^N \frac{\alpha_i \rho_i \beta_i}{1 + \beta_i^2}, \quad (17)$$

where the Hall parameter for species  $i$  is given by

$$\beta_i = \frac{\alpha_i B}{K_{1i} \rho_1}. \quad (18)$$

### 3 NUMERICAL APPROACH

#### 3.1 The gas equations

Assuming a piecewise constant solution at time  $t^n$  on a uniform mesh of spacing  $h$ , the solution at a later time  $t^{n+1} = t^n + \tau$  is sought. The state in cell  $j$  represents the volume average over  $(j - 1/2)h \leq x \leq (j + 1/2)h$ .

It should first be noted that the charged particle pressures<sup>1</sup> and velocities ( $p_i^{n+1}$  and  $q_i^{n+1}$  for  $i > 1$ ) can be obtained algebraically through equations (5) and (6). This procedure is described in Appendix A.

To obtain the full solution at time  $t^{n+1}$ , finite volume methods are applied to equations (1) to (8). The time integration is multiplicatively operator split into five operations, with each carried out to second order accuracy in space and time. The order is permuted over successive timesteps such that second order temporal accuracy is maintained over the full step (Strang 1968). In the following the five necessary operations for finite volume integration are described.

(i) Equations (1) to (3) (with  $i = 1$  for the mass equation) form a system of equations for the neutral gas. Working in terms of the primitive variables  $\mathbf{P} = (\rho_1, \mathbf{q}_1, p_1)^T$ , fluxes are evaluated from a piecewise constant solution  $\mathbf{P}^n$  via a hydrodynamic Riemann solver. A time centred solution,  $\mathbf{P}^{n+1/2}$ , obtained from these fluxes is then reconstructed to a second order piecewise-linear solution,  $\bar{\mathbf{P}}^{n+1/2}$ , using Van Albada nonlinear averaging for the gradients. Fluxes may then be derived from  $\bar{\mathbf{P}}^{n+1/2}$  which are second order accurate in space and time (for further details see, for example, Falle 1991). These fluxes are then applied to the conserved variables.

(ii) The source terms on the right hand sides of equations (2) and (3) are applied.

(iii) The charged particle mass fluxes are applied using equation (1) with  $i > 1$  in a second order upwind procedure similar to that used for the neutral gas.

(iv) The hyperbolic flux on the left hand side of equation (4) is applied via a centred approximation

$$\mathbf{M}_{j+1/2} = \frac{1}{2} (\mathbf{M}_{j+1} + \mathbf{M}_j). \quad (19)$$

This has the disadvantage of not coupling the bulk fluid to the magnetic field through a Riemann problem, however, it is necessary in order that purely hydrodynamic subshocks may be properly captured. As remarked by F03, as long as the magnetic field appears continuous on the grid, as should be the case with finite resistivities, this is perfectly acceptable.

(v) The resistive term on the right hand side of equation (4) is applied. Discussion of this procedure is deferred to the following section since it is of special interest.

<sup>1</sup> It is actually the charged species' temperatures which are derived as their pressures are not explicitly necessary under the assumptions made here.

#### 3.2 Magnetic diffusion

Splitting the hyperbolic flux term  $\partial \mathbf{M} / \partial x$  from the induction equation (4) and linearising yields

$$\frac{\partial \mathbf{B}}{\partial t} = \mathbf{R} \frac{\partial^2 \mathbf{B}}{\partial x^2}. \quad (20)$$

Note that the linearised form is assumed for convenience in the following analysis and in practise generalised discretisations of the nonlinear diffusion term are used.

##### 3.2.1 Standard discretisation

The usual explicit discretisation for a diffusion term applied to equation (20) yields

$$\mathbf{B}_j^{n+1} = \mathbf{B}_j^n + \frac{\tau}{h^2} \mathbf{R}_j^n (\mathbf{B}_{j+1}^n - 2\mathbf{B}_j^n + \mathbf{B}_{j-1}^n) \quad (21)$$

Assuming  $r_O$  to be negligible, the relative importance of the remaining resistivities can be parameterised by  $\eta \equiv r_A / |r_H|$ . F03 showed the above scheme has an amplification matrix with eigenvalues which are real when  $\eta \geq \eta^*$  and complex otherwise. The transition point  $\eta^*$  is given by

$$\eta^* = 2|\cos\theta| / \sin^2\theta \quad (22)$$

where  $\theta$  is the pitch angle of the field with respect to the  $x$ -axis. In the real regime, the stability limit on the timestep is

$$\bar{\tau}^R = \frac{2\sqrt{1 + \eta^2}}{\eta(1 + \cos^2\theta) + 2|\cos\theta|\sqrt{(\eta/\eta^*)^2 - 1}} \quad (23)$$

where  $\bar{\tau} \equiv \tau / \tau^\perp$  and  $\tau^\perp$  is the characteristic cell crossing time for diffusion perpendicular to the magnetic field given by

$$\tau^\perp = \frac{h^2}{2|r_H| \sqrt{1 + \eta^2}}. \quad (24)$$

However, below the transition point the stability limit becomes

$$\bar{\tau}^C = \frac{1 + \cos^2\theta}{2\cos^2\theta} \frac{\eta}{\sqrt{1 + \eta^2}}. \quad (25)$$

In either case the stable timestep limit goes as  $h^2$  since this is an explicit discretisation of a diffusion equation, however, a potentially more severe constraint is that while this limit increases as  $\eta \rightarrow \eta^*$  in the real regime, it rapidly drops to zero as  $\eta \rightarrow 0$  in the complex regime.

##### 3.2.2 Numerical Strategy

Our strategy is to split  $r_H$  into two parts such that

$$r_H = r_H^a + r_H^b \quad (26)$$

where  $r_H^a \equiv \frac{\eta}{\eta^*} r_H$  is the maximum allowable Hall resistivity in the real regime and  $r_H^b$  is the excess. The induction

equation is then integrated in two parts using a technique to accelerate the timestepping for the standard discretisation with Hall resistivity  $r_H^a$ . The excess Hall resistivity  $r_H^b$  is then applied using a different discretisation with suitable stability properties.

### 3.2.3 Super Time Stepping

STS is a technique which can be used to accelerate explicit schemes for parabolic problems. Essentially a Runge-Kutta-Chebyshev method, it has been known for some time (see Alexiades, Amiez & Gremaud 1996), although it remains relatively unknown in computational astrophysics.

A superstep  $\tau^{\text{STS}}$  is a composite timestep built up from a series of  $N_{\text{STS}}$  substeps such that

$$\tau^{\text{STS}} = \sum_{j=1}^{N_{\text{STS}}} d\tau_j. \quad (27)$$

Judicious choice of the  $d\tau_j$  yields stability for the superstep while the normal stability restrictions on the individual substeps are relaxed. Exploiting the properties of Chebyshev polynomials provides a set of optimal values for the substeps given by

$$d\tau_j = \tau^X \left[ (-1 + \nu) \cos \left( \frac{2j - 1}{N_{\text{STS}}} \frac{\pi}{2} \right) + 1 + \nu \right]^{-1} \quad (28)$$

where  $\tau^X$  is the normal explicit timestep limit and  $\nu$  is a damping factor. Note that  $\tau^{\text{STS}} \rightarrow N_{\text{STS}}^2 \tau^X$  as  $\nu \rightarrow 0$ . The method is unstable in the limit  $\nu = 0$ . For a more detailed discussion, see Alexiades, Amiez & Gremaud (1996) and references therein.

In order to apply STS to second order in time Richardson extrapolation is used.

### 3.2.4 Hall Diffusion Scheme

Having advanced the induction equation with a Hall resistivity  $r_H^a$ , it is necessary to find an efficient scheme to impose the excess Hall diffusion  $r_H^b$ . Since multiplicative operator splitting yields a composite scheme with an amplification factor equal to the product of the amplification factors of the basis schemes this task can be reduced to one of finding a scheme for pure Hall diffusion.

The key observation to make is that  $\mathbf{R}$  has zero entries on the diagonal when pure Hall diffusion is being considered. With this in mind, equation (21) may be used to advance one component of the magnetic field explicitly, followed by an implicit-like discretisation of the alternate component. We call this the Hall Diffusion Scheme (HDS) as we are not aware of an instance of this approach elsewhere in the literature. Hence the discretisation of equation (21) for the pure Hall excess  $r_H^b$  becomes

$$B_{y,j}^{n+1} = B_{y,j}^n + \frac{\tau}{h^2} d_H^b (B_{z,j+1}^n - 2B_{z,j}^n + B_{z,j-1}^n) \quad (29)$$

followed by

$$B_{z,j}^{n+1} = B_{z,j}^n - \frac{\tau}{h^2} d_H^b (B_{y,j+1}^{n+1} - 2B_{y,j}^{n+1} + B_{y,j-1}^{n+1}) \quad (30)$$

where the cosine term is absorbed by defining  $d_H^b = r_H^b \cos \theta$ . It seems to make little difference which component is advanced first.

For clarity of notation the superscript  $b$  is dropped from the following analysis of the stability properties of the scheme. The resistance matrix for pure Hall diffusion is

$$\mathbf{R} = \begin{pmatrix} 0 & d_H \\ -d_H & 0 \end{pmatrix}. \quad (31)$$

Assuming a numerical wave of the form

$$\mathbf{B}_j^n = \mathbf{B}^n e^{i\omega j} \quad (32)$$

in equations (29) and (30) yields an amplification matrix

$$\mathbf{A} = \begin{pmatrix} 1 & -\hat{d}_H \\ \hat{d}_H & 1 - \hat{d}_H^2 \end{pmatrix} \quad (33)$$

where  $\hat{d}_H \equiv \xi d_H$  and

$$\xi = \frac{2\tau(1 - \cos \omega)}{h^2}. \quad (34)$$

The eigenvalues of  $\mathbf{A}$  are given by

$$\lambda = 1 - \frac{1}{2} \hat{d}_H^2 \pm i \frac{1}{2} \hat{d}_H \sqrt{4 - \hat{d}_H^2} \quad (35)$$

and hence HDS is neutrally stable for  $|\hat{d}_H| \leq 2$ . Taking the most restrictive case of  $\omega = \pi$  gives a stable timestep limit of

$$\bar{\tau}^{\text{HDS}} = \frac{\sqrt{1 + \eta^2}}{|\cos \theta| (1 - \eta/\eta^*)}. \quad (36)$$

Note that  $\bar{\tau}^{\text{HDS}} \rightarrow 1/|\cos \theta|$  as  $\eta \rightarrow 0$  in contrast to the standard discretisation for which  $\bar{\tau}^{\text{C}} \rightarrow 0$ .

The extension of the HDS to more than one dimension is straightforward although we defer a detailed discussion to a later paper. For an outline of the scheme in three dimensions the reader is referred to Appendix B.

In practice, ordinary (unaccelerated) subcycling of HDS, using  $N_{\text{HDS}}$  subcycles, is applied in conjunction with STS. This compound scheme (referred to as ‘‘STS/HDS’’ hereafter) usually allows the timestep limit imposed by the hyperbolic terms to be reached efficiently (see Subsection 4.4).

## 4 NUMERICAL TESTS

Following F03, the dynamic algorithm described here is tested against solutions of the steady isothermal multifluid equations. These steady state equations are solved using an independent code, the details of which are outlined in Appendix C. The conditions for each of the tests are given in Table 1.

### 4.1 Case A: Ambipolar Dominated

In this test  $r_O = 2 \times 10^{-12}$ ,  $r_H = 1.16 \times 10^{-5}$  and  $r_A = 0.068$  giving  $\eta = 5.86 \times 10^3$  and hence it can be expected that ambipolar diffusion will dominate the solution. Fig. 1 shows plots of the  $x$  component of the neutral velocity, along with  $B_y$  for both the dynamic and steady state solutions. The calculation shown has  $h = 5 \times 10^{-3}$ . It can be seen that the agreement between the two solutions is extremely good.

Case A					
Right State	$\rho_1 = 1$	$\mathbf{q}_1 = (-1.751, 0, 0)$	$\mathbf{B} = (1, 0.6, 0)$	$\rho_2 = 5 \times 10^{-8}$	$\rho_3 = 1 \times 10^{-3}$
Left State	$\rho_1 = 1.7942$	$\mathbf{q}_1 = (-0.9759, -0.6561, 0)$	$\mathbf{B} = (1, 1.74885, 0)$	$\rho_2 = 8.9712 \times 10^{-8}$	$\rho_3 = 1.7942 \times 10^{-3}$
	$\alpha_2 = -2 \times 10^{12}$	$\alpha_3 = 1 \times 10^8$	$K_{21} = 4 \times 10^5$	$K_{31} = 2 \times 10^4$	$a = 0.1$
	$\nu = 0.05$	$N_{STS} = 5$	$N_{HDS} = 0$		
Case B					
Right State	As case A				
Left State	As case A				
	$\alpha_2 = -2 \times 10^9$	$\alpha_3 = 1 \times 10^5$	$K_{21} = 4 \times 10^2$	$K_{31} = 2.5 \times 10^6$	$a = 0.1$
	$\nu = 0$	$N_{STS} = 1$	$N_{HDS} = 8$		
Case C					
Right State	$\rho_1 = 1$	$\mathbf{q}_1 = (-6.7202, 0, 0)$	$\mathbf{B} = (1, 0.6, 0)$	$\rho_2 = 5 \times 10^{-8}$	$\rho_3 = 1 \times 10^{-3}$
Left State	$\rho_1 = 10.421$	$\mathbf{q}_1 = (-0.6449, -1.0934, 0)$	$\mathbf{B} = (1, 7.9481, 0)$	$\rho_2 = 5.2104 \times 10^{-7}$	$\rho_3 = 1.0421 \times 10^{-2}$
	$\alpha_2 = -2 \times 10^{12}$	$\alpha_3 = 1 \times 10^8$	$K_{21} = 4 \times 10^5$	$K_{31} = 2 \times 10^4$	$a = 1$
	$\nu = 0.05$	$N_{STS} = 15$	$N_{HDS} = 0$		

**Table 1.** Test calculation parameters.

Since the algorithm is designed to be second order it is worthwhile measuring the convergence rate of the dynamic solution against the solution from the steady state solver. The comparison is made by minimising the L1 error norm,  $e_1$ , between a section of the dynamical solution and the steady state solution. Working from the downstream side, the section  $x_L \leq x \leq x_R$  is fixed about the point  $x^*$  where the deviation from the downstream state first exceeds 50% of the maximum variation in the solution. Using  $x_L = x^* - 0.44$  and  $x_R = x^* + 0.56$  yields  $e_1 = 3.90 \times 10^{-5}$  for  $h = 5 \times 10^{-3}$ , and  $e_1 = 1.56 \times 10^{-4}$  for  $h = 1 \times 10^{-2}$ . This gives  $e_1 \propto h^{2.0}$  – showing second order convergence as expected.

#### 4.2 Case B: Hall Dominated

The Hall term dominates in this test, requiring the Hall diffusion to be split and applied in part via HDS. The parameters are  $r_O = 2 \times 10^{-9}$ ,  $r_H = 0.0116$ ,  $r_A = 5.44 \times 10^{-4}$  with  $\eta = 0.0046 \ll 1$ .<sup>2</sup> Fig. 2 shows the results of the calculations for the test with  $h = 2 \times 10^{-3}$ . For standard explicit codes the conditions lead to prohibitive restrictions on the timestep. However, the use of HDS allows us to maintain a timestep close to the Courant limit imposed by the hyperbolic terms throughout the calculations.

As with case A, the dynamic solution is tested to ensure it has the correct second order convergence characteristics. With  $x_L = x^* - 0.15$  and  $x_R = x^* + 0.95$ , we find  $e_1 = 4.95 \times 10^{-3}$  for  $h = 2 \times 10^{-3}$  and  $e_1 = 1.15 \times 10^{-3}$  for  $h = 1 \times 10^{-3}$ , giving  $e_1 \propto h^{2.1}$ . Again, this is close to the second order convergence rate expected.

#### 4.3 Case C: Neutral subshock

This test is similar to case A, but with a higher soundspeed and upstream fast Mach number. As a result, a subshock develops in the neutral flow because the interactions between the charged particles and the neutrals are not strong enough to completely smooth out the strong initial discontinuity in

<sup>2</sup> If the Hall diffusion is increased much further, it appears that the approximation of negligible charged particle inertia breaks down.

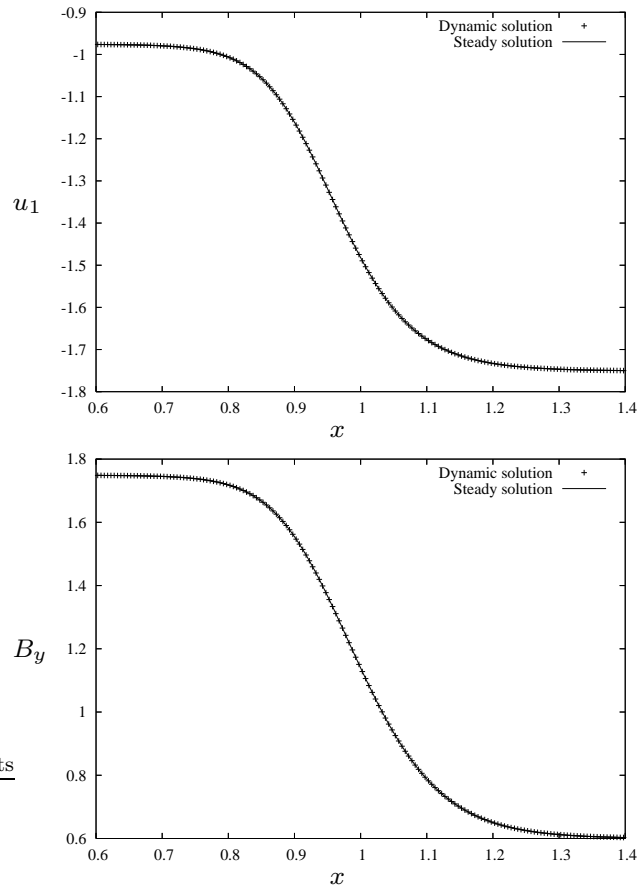


**Figure 1.** Neutral fluid  $x$ -velocity and  $y$ -component of magnetic field for case A with  $h = 5 \times 10^{-3}$ . The solution from the steady state equations, as a line, is overplotted with points from the dynamic code.

the neutral flow. The ability of the algorithm described to deal with discontinuities in the solution is therefore tested.

Fig. 3 shows the results of the calculations for  $h = 1 \times 10^{-3}$ . The subshock in the neutral flow is clearly visible as a discontinuity in  $u_1$ , while there is no corresponding discontinuity in  $B_y$ . Fig. 4 contains a plot of the  $x$  component of the velocity of the negatively charged fluid. As expected,

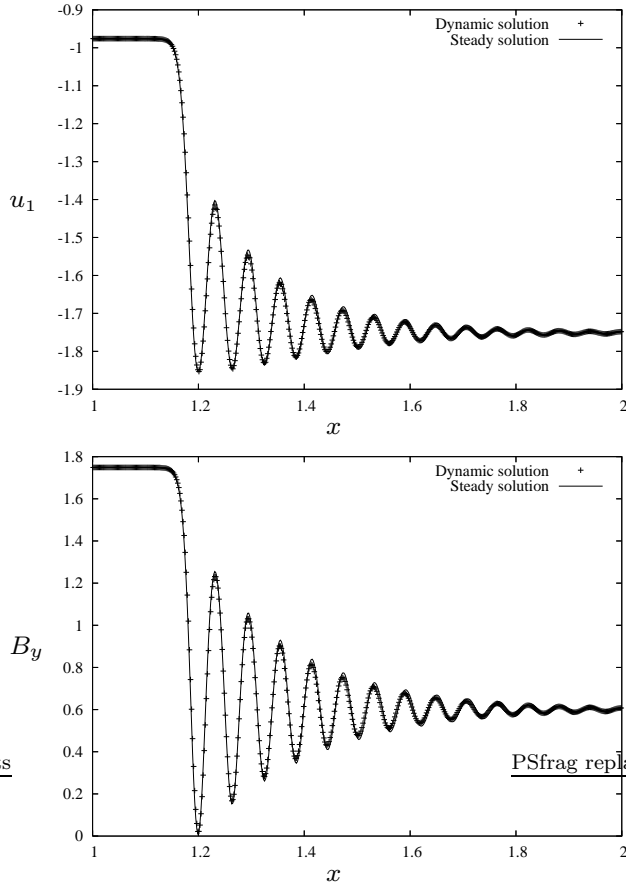


**Figure 2.** Neutral fluid  $x$ -velocity and  $y$ -component of magnetic field for case B with  $h = 2 \times 10^{-3}$ . The solution from the steady state equations, as a line, is overplotted with points from the dynamic code.

there is no discontinuity in this variable, but there are some oscillations at the point where the discontinuity in the neutral flow occurs. These errors are remarkably similar to those encountered by F03 and do not affect the global solution.

It can be expected that, since there is a discontinuity in the solution of this test and a MUSCL-type approach is used, the rate of convergence of the dynamic solution will be close to first order, at least for resolutions high enough to discern the subshock in the solution. In this test  $x_L = x^* - 0.13$  and  $x_R = x^* + 0.15$ . We find  $e_1 = 3.41 \times 10^{-2}$  for  $h = 5 \times 10^{-3}$  and  $e_1 = 5.25 \times 10^{-3}$  for  $h = 1 \times 10^{-3}$  yielding  $e_1 \propto h^{1.16}$  – close to the first order expected, although clearly the error from around the subshock is not completely dominating at this resolution. At  $h = 5 \times 10^{-4}$  we find  $e_1 = 2.73 \times 10^{-3}$  giving  $e_1 \propto h^{0.94}$  with respect to the error at  $h = 1 \times 10^{-3}$ . We suspect that the deviation from first order is due to a discontinuity in the electric field at the subshock causing an error in the charged velocities since smoothing the solution with some artificial viscosity is found to improve the convergence.

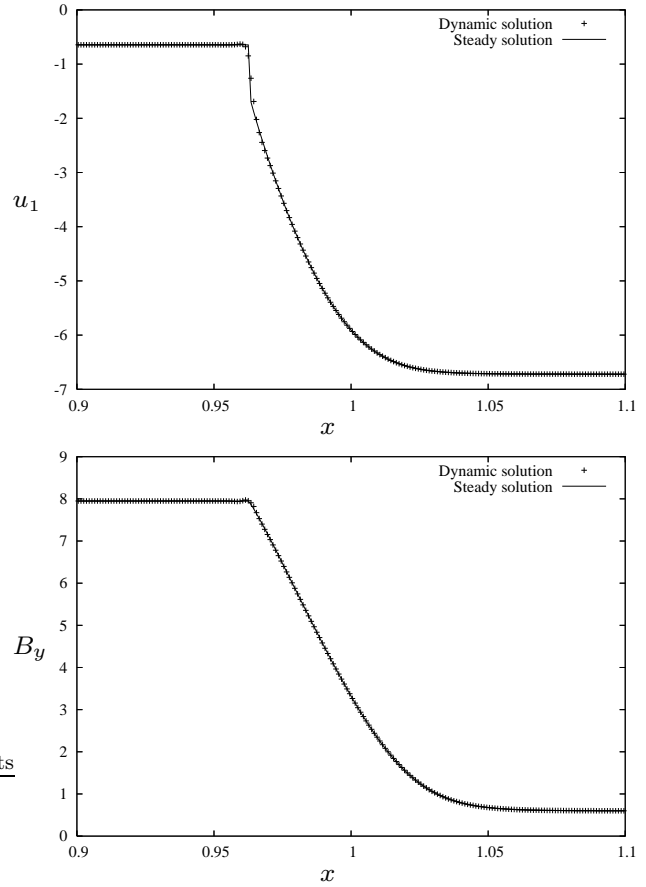


**Figure 3.** Neutral fluid  $x$ -velocity and  $y$ -component of magnetic field for case C with  $h = 1 \times 10^{-3}$ . The solution from the steady state equations, as a line, is overplotted with points from the dynamic code.

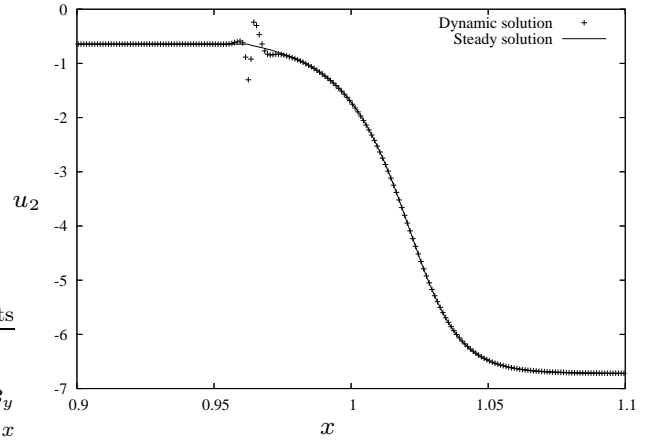


**Figure 4.** Negatively charged fluid  $x$ -velocity for case C with  $h = 1 \times 10^{-3}$ . The solution from the steady state equations, as a line, is overplotted with points from the dynamic code.

	Case A	Case B	Case C
STS/HDS	1.9	14.8	1.9
Implicit	1.9	23.3	2.7

**Table 2.** The speed-up factors in CPU time usage achieved via the implicit and STS/HDS discretisations of the induction equation relative to the standard explicit discretisation.

#### 4.4 Comparative timings

In this section comparison is made between the performances of standard explicit, STS/HDS, and implicit (Crank-Nicolson) discretisations of the induction equation. The different methods are applied in otherwise identical codes to the high resolution trials of the preceding test cases. Since the neutral gas equations are treated explicitly in all cases, the corresponding Courant condition on the integration of the hyperbolic terms imposes a hard limit on the timestep.

As a benchmark, we use the standard explicit discretisation subcycled to the same degree as the STS/HDS method. The speed-up factors of the STS/HDS and implicit methods in terms of CPU time usage are presented in Table 2. Clearly, either technique offers a significant improvement in efficiency and both achieve timesteps close to the limit introduced by the hyperbolic terms. The implicit method is slightly faster for case C due to the high degree of subcycling used for the STS and significantly so for case B because of the very large Hall term. Otherwise, the STS/HDS and implicit methods yield similar speed-up factors indicating that overall efficiency is dominated by the other parts of the schemes. It should be emphasised that these are steady state problems which suit implicit methods particularly well and for non-steady state problems accuracy constraints may reduce the efficiency of implicit schemes.

## 5 CONCLUSIONS

A new explicit scheme for integrating the multifluid equations in the limit of low ionisation has been presented. The usual explicit stability limit imposed by the induction equation is relaxed by means of the Super Time Stepping algorithm applied for a portion of the Hall diffusion up to a critical limiting value.

Beyond this limiting value the standard explicit discretisation becomes subject to a stability constraint requiring that the timestep vanish as the Hall diffusion becomes large. In order to circumvent this constraint, the excess Hall diffusion above the critical value is split off and applied via a new method which we have called the Hall Diffusion Scheme.

It has been demonstrated that, for the case of an isothermal flow, the algorithm is accurate and converges to second order when the solution is smooth and to first order when the solution contains a discontinuity. The extension of this scheme to non-isothermal flow does not present any obvious difficulties, although a modification of the discretisation used for the magnetic flux evolution is necessary.

Since all discretisations used in the scheme presented here are explicit, it is a straightforward matter to implement in a multidimensional parallelised codes using adaptive mesh refinement. This is a crucial advantage for large-scale sim-

ulations of astrophysical systems in which multifluid effects are thought to be important such as dense molecular clouds and protostellar accretion disks.

## ACKNOWLEDGEMENTS

This work was partly funded by the CosmoGrid project, funded under the Programme for Research in Third Level Institutions (PRTLI) administered by the Irish Higher Education Authority under the National Development Plan and with partial support from the European Regional Development Fund.

The authors are grateful to the School of Cosmic Physics at the Dublin Institute for Advances Studies for facilitating this collaboration and to the referee Sam Falle for valuable comments.

## REFERENCES

Alexiades V., Amiez G., Gremaud P., 1996, Com. Num. Meth. Eng., 12, 31  
 Chieze J.-P., Pineau des Forets G., Flower D.R., 1998, MNRAS, 295, 672  
 Ciolek G.E., Roberge, W.G., 2002, ApJ, 567, 947 (CR02)  
 Falle S.A.E.G., 1991, MNRAS, 250, 581  
 Falle S.A.E.G., 2003, MNRAS, 344, 1210 (F03)  
 Fendt, C., Camenzind, M., 1996, A&A, 313, 591  
 Ferreira J., 2004, ApSS, 293, 83  
 Hollerbach R., Rüdiger G., 2004, MNRAS, 347, 1273  
 Lery, T., Heyvaerts, J., Appl., S., Norman, C.A., 1999, A&A, 347, 1055  
 Ouyed, R., Pudritz, R.E., Stone, J.M., Nature, 385, 409  
 Sano T., Stone J.M., 2002a, ApJ, 570, 314  
 Sano T., Stone J.M., 2002b, ApJ, 577, 534  
 Shu, F., Najita, J., Ostriker, E., Wilkin, F., Ruden, S., Lizano, S., 1994, ApJ, 429, 781  
 Smith M.D., Mac Low, M.-M., 1997, A&A, 326, 801  
 Stone J.M., 1997, ApJ, 487, 271  
 Strang G., 1968, SIAM J. Numer. Anal., 5, 505  
 Tóth G., 1994, ApJ, 425, 171  
 Wardle M., 1991, MNRAS, 251, 119  
 Wardle M., 2004, ApSS, 292, 317

## APPENDIX A: CHARGED VELOCITIES

For this work the collisional coefficients  $K_{i1}$  are assumed to be independent of velocities and temperatures. The following derivation (S.A.E.G. Falle, private communication) is included for completeness.

Transforming to the frame co-moving with the neutral gas, equation (5) can be written as

$$\mathbf{q}'_i \times \mathbf{B} - \kappa_i \mathbf{q}'_i = -\mathbf{E}' - \mathbf{q}_1 \times \mathbf{B} \quad (\text{A1})$$

where  $\kappa_i \equiv \rho_1 K_{i1} / \alpha_i$  and  $\mathbf{E}' = \mathbf{E} + \mathbf{q}_1 \times \mathbf{B}$ .

Then choosing  $i = 2$  as a reference species, the general

solutions for the remaining charged species' velocities are given by

$$\mathbf{q}'_i = \mathbf{A}_i^{-1} \mathbf{A}_2 \mathbf{q}'_2 \quad (\text{A2})$$

where

$$\mathbf{A}_i = \begin{pmatrix} -\kappa_i & B_z & -B_y \\ -B_z & -\kappa_i & B_x \\ B_y & -B_x & -\kappa_i \end{pmatrix}. \quad (\text{A3})$$

To derive the charged velocities, all that remains is for the reference velocity to be evaluated, this can be done by using equation (9) and Ampère's law to give

$$\mathbf{q}'_2 = \left[ \mathbf{I} - \left( \sum_{i=3}^N \frac{\alpha_i \rho_i}{\alpha_2 \rho_2} \mathbf{A}_i^{-1} \right) \mathbf{A}_2 \right]^{-1} \frac{\nabla \times \mathbf{B}}{\alpha_2 \rho_2}. \quad (\text{A4})$$

If the collisional coefficients are in fact dependent on the velocities of the charged species, this procedure can be carried out iteratively using the values from the previous timestep as a starting point.

Should the collisional coefficients depend on the temperatures of the charged species, some additional calculation is necessary before the next iteration: using equation (6) and inserting the specific form of the function  $G_{i1}$ ,  $N - 1$  equations are obtained which may be solved readily for the  $N - 1$  charged temperatures.

Finally, it is worth noting that superior results are obtained by interpolating the primitive quantities to the cell edges before calculating the charged velocities rather than by calculating the velocities at the cell centres and interpolating from these to the edges.

## APPENDIX B: HDS IN THREE DIMENSIONS

Equation (5) can be used in conjunction with equation (9) to write the electric field for pure Hall diffusion as

$$\mathbf{E} = r_H \frac{\mathbf{J} \times \mathbf{B}}{B} \quad (\text{B1})$$

Then, using Faraday's law, we can write

$$\frac{\partial \mathbf{B}}{\partial t} = -r_H \nabla \times (\mathbf{J} \times \mathbf{b}) \quad (\text{B2})$$

where  $\mathbf{b} \equiv \mathbf{B}/B$ .

This equation can be expanded out and linearised to give

$$\frac{\partial \mathbf{B}}{\partial t} = \mathbf{G} \mathbf{B} \quad (\text{B3})$$

where, using  $\mathbf{J} = \nabla \times \mathbf{B}$ , the matrix  $\mathbf{G}$  is given by

$$\mathbf{G} = -r_H (\mathbf{b} \cdot \nabla) \nabla \times . \quad (\text{B4})$$

Hence  $\mathbf{G}$  is antisymmetric and we can write the generalised HDS scheme as

$$B_x^{n+1} = B_x^n + \tau(G_{x y}^n B_y^n + G_{x z}^n B_z^n), \quad (\text{B5})$$

$$B_y^{n+1} = B_y^n + \tau(G_{y z}^n B_z^n + G_{y x}^n B_x^{n+1}), \quad (\text{B6})$$

$$B_z^{n+1} = B_z^n + \tau(G_{z x}^n B_x^{n+1} + G_{z y}^n B_y^{n+1}), \quad (\text{B7})$$

where  $\mathbf{G}^n$  is the discretised form of the operator  $\mathbf{G}$  at time level  $n$ .

The generalised HDS scheme in three dimensions is analogous in construction to the one-dimensional case in that equation (B5) is an explicit first step and equation (B7) is an implicit-like final step. Additionally, we now have an intermediate step of mixed explicit/implicit character. Numerical tests indicate that the method retains its favourable stability properties in three dimensions.

## APPENDIX C: STEADY-STATE SOLVER

Assuming an isothermal flow, as is the case for the tests presented in this work, setting all derivatives with respect to time to zero in the multifluid equations gives us

$$\rho_i u_i = Q_i = \text{constant}, \quad (\text{C1})$$

$$\rho_1 u_1^2 + a^2 \rho_1 + \frac{B^2}{2} = P_x = \text{constant}, \quad (\text{C2})$$

$$\rho_1 u_1 v_1 - B_x B_y = P_y = \text{constant}, \quad (\text{C3})$$

$$\rho_1 u_1 w_1 - B_x B_z = P_z = \text{constant}. \quad (\text{C4})$$

In addition the reduced momentum equations for the charged species (equation (5)) yield 3 equations for each charged species, and the charge neutrality condition is also used. Finally, the equation for  $\mathbf{B}$  yields

$$\mathbf{M} - \mathbf{M}_R = \mathbf{R} \frac{d\mathbf{B}}{dx} \quad (\text{C5})$$

with  $\mathbf{M}_R$  ( $= \mathbf{M}_L$ ) being the flux in the right (left) state.

For the cases considered here, with two charged species, the above equations constitute one ordinary differential equation for  $\mathbf{B}$  and seven equations which, once  $\mathbf{B}$  is known at a given point in space, can be used to solve for all the other variables. The ODE for  $\mathbf{B}$  is solved using the Runge-Kutta method of order 4.

The initial conditions (at  $x = 0$ ) are a saddle point of the ODE for  $\mathbf{B}$ . These conditions are perturbed slightly and the system then evolves through phase space to a sink point.